A High-Power, High-Frequency Matrix Core Transformer Design for Medium Voltage Dual Active Bridge

Zhe Zhao, Yuheng Wu, Fei Diao, Nan Lin, Xinyuan Du, and Yue Zhao
Department of Electrical Engineering
University of Arkansas
Fayetteville, AR, 72701 USA
zhezhao@uark.edu, yuhengwu@uark.edu, feidiao@uark.edu, nl005@uark.edu, xd006@uark.edu, yuezhao@uark.edu

***Abstract*—In this work, the analytical models and optimization procedure for the design of high-power matrix core transformer (MCT) aiming at isolated DC/DC converter applications, especially for dual active bridge (DAB) converters, are proposed. The loss models, leakage inductance and thermal network models of MCT are presented, and a multi-variable, multi-objective optimization methodology of MCT is proposed. A 100 kW/50 kHz MCT design is selected and prototyped based on the optimization results. An additive manufactured bobbin design is also presented to control the leakage inductance and the path of the airflow. The electrical, magnetic, and thermal performance of the prototype are validated using by experimental studies.**

Keywords—High-frequency Transformer (HFT), Dual Active Bridge (DAB), Isolated DC/DC Converter.

I. INTRODUCTION

Solid-state transformer (SST) is considered as an attractive solution for medium voltage (MV) power transmission [1]. There exists much research discussed the developments of SST in various application such as future data centers power supply, renewable energy system and traction equipment [2-4]. The main principle of SST is to use high-frequency isolated transformer (HFT) instead of line-frequency transformer (LFT), which significantly reduces the volume and weight of the system [5]. SST can be classified into a few types, and dual active bridge (DAB) is a commonly used converter for high power operation among them [6]. The topology of typical DAB is shown in Fig. 1, which contains two H-bridges for DC/AC and AC/DC conversion, and one HFT for AC/AC power flow and galvanic isolation. The voltage and power of DAB is regulated with the phase shift between the control signals on both H-bridges. In the HFT, the leakage inductance L_σ influences the power level and the soft-switching realization, and the magnetizing inductance L_m should be designed as large as possible to decrease the effect of magnetizing current [7]. With high power operation, the core and winding losses can lead to lower efficiency, and the compact structure for high power density requires accurate and effective cooling design. As a result, it is still a challenging task for the HFT design.

There are several considerable approaches for the high-power HFT optimization. Accurate leakage and thermal models for shell-type transformer are discussed in [8] and applied on a 100 kW/10 kHz HFT prototype design. [9] presents the application of both the water-cooling system design and nanocrystalline cores on a 166 kW/20 kHz HFT design. A 200 kW/15 kHz HFT prototype with high isolation capability is shown in [10]. However, there are still demands of higher power and higher frequency HFT, and in this paper, a 100 kW, 50 kHz matrix core transformer (MCT) is designed based on proposed analytical models and optimization methodology, which is lacking in previous research.

This work was supported by in part by the U.S. National Science Foundation (NSF) Center on Grid Connected Advanced Power Electronic Systems (GRAPES) under Grant 1939144.

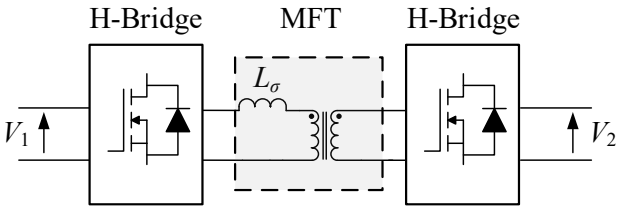

Fig. 1. Topology of DAB with two H-bridges and one MFT.

In this paper, the modeling, design, and optimization of MCT are focused on, and a 100 kW/50 kHz MCT prototype is built and tested. The losses, leakage inductance, and thermal models of MCT are introduced in detail in Section II, and a high-power MCT is optimally designed from the optimization methodology in Section III. The prototype with a 3D-print bobbin is presented and its performance is verified by experimental results in Section IV. The final conclusions are illustrated in Section V.

II. ANALYTICAL MODELS OF MCT

The structure of MCT is shown in Fig. 2 [11]. Compared with traditional shell-type transformer, MCT has a circular winding arrangement and split cores. The windings are typed into inside the core window (IW) part and outside the core window (OW) part. The gap between two windings is functional as the leakage inductance control and airflow cooling channel.

A. Loss Evaluation

In order to estimate the core loss, the improved generalized Steinmetz equation (IGSE) is proved to have high accuracy, especially for the square waveform voltage excitation of DAB [12]. Based on the Steinmetz coefficients K, α and β, the core loss per unit volume is expressed as

$$P_c = 2^{\alpha+\beta} K_i f^\alpha B_m^\beta \tag{1}$$

in IGSE, where

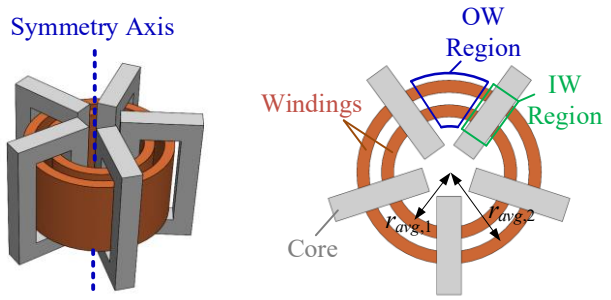

Fig. 2. The structure of MCT (left) and the top view (right).

$$K_i = \frac{K}{2^{\beta-1}\pi^{\alpha-1}\int_0^{2\pi}|\cos\theta|\mathrm{d}\theta} \tag{2}$$

The ferrite cores are selected since the frequency reaches 50kHz, and the eddy current loss of nanocrystalline cores increases significantly.

Due to the skin effect and proximity effect, the winding loss worsens as the frequency rises. A classic formula for winding loss estimation was proposed by Dowell [13], and Wojda generalized it for high frequency rectangle litz wires with the approximate formula given by

$$F_r \approx 1+\frac{5m^2k-1}{45}A_{str}^4 \tag{3}$$

where F_r is the ac-to-dc winding resistance ratio, m is the number of layers, k is the number of strands in one bundle, and A_{str} is the effective diameter of the strand in [14]. Considering the winding current is non-sinusoidal waveform, the fast Fourier transform is needed to obtain the current harmonics distribution, and the final winding loss is calculated as

$$P_w = R_{\mathrm{dc}}\sum_{n=1}^{\infty} I_n^2 F_{rn} \tag{4}$$

where R_{dc} is the dc winding resistance, I_n and F_m are the root mean square (RMS) value of current component and the value of F_r in nth frequency range, respectively.

B. Leakage Inductance

The power level of DAB converter under single phase shift (SPS) modulation can be derived as

$$P = \frac{nV_1V_2}{2\pi^2 f_s L_\sigma}\varphi(\pi-\varphi) \tag{5}$$

where n is the turns-ratio of the transformer, V_1 and V_2 are the input and output voltage, respectively, f_s is the switching frequency, and φ is the phase shift. It can be seen that the leakage inductance L_σ influences the delivered power, thus it should be designed accurately. Even though the auxiliary inductor can be used to satisfy the requirement, the power density is decreased.

The ideal solution is to control the leakage inductance in the design procedure of the transformer. Since the leakage inductance is generated by the flux uncoupled both windings, a popular approach to estimate the leakage inductance is to calculate the leakage energy E stored within the windings and the winding gap with the magnetomotive force (MMF) as

$$L_\sigma = \frac{2E}{I^2} = \frac{\mu_0}{I^2}\int_V H^2 dV \tag{6}$$

where μ_0 is the permeability of the air, H is field strength, and V is the total volume of space [15]. From the cross-section of MCT and the analytical MMF distribution shown in Fig. 3, the integral term in (6) can be calculated as

$$\begin{aligned}\int_V H^2 dV &= 2\pi r_w\left[\begin{array}{l}\int_0^{D_{w1}}\left(\frac{I}{h_w}\frac{x}{D_{w1}}\right)^2\mathrm{d}x \\ +\int_0^{D_\sigma}\left(\frac{I}{h_w}\right)^2\mathrm{d}x \\ +\int_0^{D_{w2}}\left(\frac{I}{h_w}\frac{x}{D_{w2}}\right)^2\mathrm{d}x\end{array}\right] \\ &= \frac{2\pi r_w I^2}{h_w}\left(\frac{D_{w1}+D_{w2}}{3}+D_\sigma\right)\end{aligned} \tag{7}$$

Substituting (7) into (6) as

$$L_\sigma = \mu_0\frac{2\pi r_w}{h_w}\left(\frac{D_{w1}+D_{w2}}{3}+D_\sigma\right) \tag{8}$$

where r_w is the radius of winding window. The accuracy of (8) is high when the frequency is lower than 100kHz since the high-frequency effects have unobvious impact on the MMF distribution [16].

C. Thermal Model

Overheat may occur within a compact high power transformer due to the lower surface area for heat dissipation,

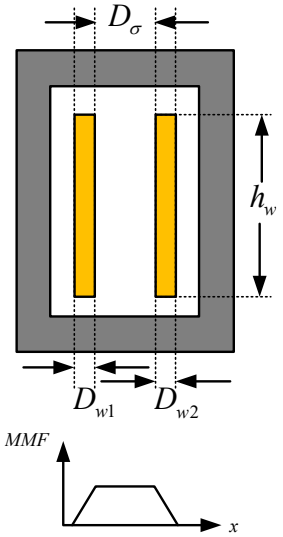

Fig. 3. Dimensions for leakage inductance estimation and MMF distribution.

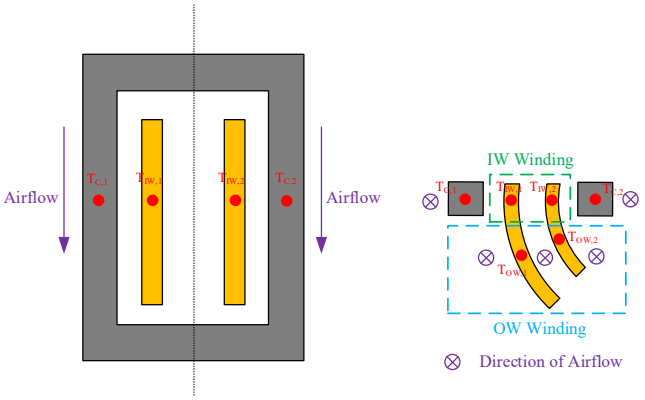

Fig. 4. Dimensions for leakage inductance estimation and MMF distribution.

and the reliability of the transformer can be decreased significantly. To overcome this difficulty, the cooling system design with accurate thermal models is required for temperature rise estimation.

From the structure of MCT, it can be seen that the split cores and OW windings have large heat radiation area, and the winding gap can provide an effective path for air flow. The thermal model of MCT is shown in Fig. 4, where the core are divided to two parts with the same core loss, and the OW winding and IW winding have different models based on their position. The thermal network of MCT is built as Fig. 5, which contains the thermal couple between the core and IW windings, between the primary and secondary windings, and between the IW and OW windings. The thermal resistance in the network are generated by the conduction, natural convection and radiation. The typical formulas to express these three heat transfer mechanisms are as follows, respectively,

$$Q_c = k\frac{A}{L}\Delta T \tag{9}$$

$$Q_{\text{conv}} = hA\left(T - T_\infty\right) \tag{10}$$

$$Q_R = \varepsilon\sigma A\left(T_1^4 - T_2^4\right) \tag{11}$$

where the parameters are shown in [17]. With the proposed thermal network, the temperature distribution of MCT can be estimated, and the hotspots are determined for the experimental thermal tests.

III. Pareto Optimization

Since there exist many design parameters in MCT, a multi-variable and multi-objective optimization methodology is needed to reach both high efficiency η and high power density ρ. The proposed MCT optimization flowchart is presented in Fig. 6, where the variables contain the core, the number of cores N_c, the current density J, the number of turns N, and the strand diameter d_{str}. The database is setup with the data of cores and litz wires. The optimization methodology starts with the waveform estimation of winding current I according to the initial parameters of power level P, voltage V, switching frequency f and required leakage

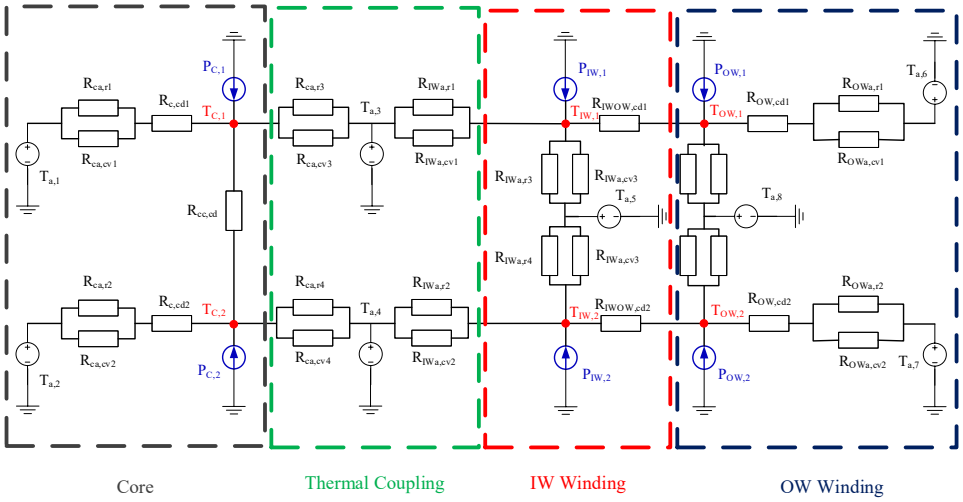

Fig. 5. Thermal network for the proposed MCT.

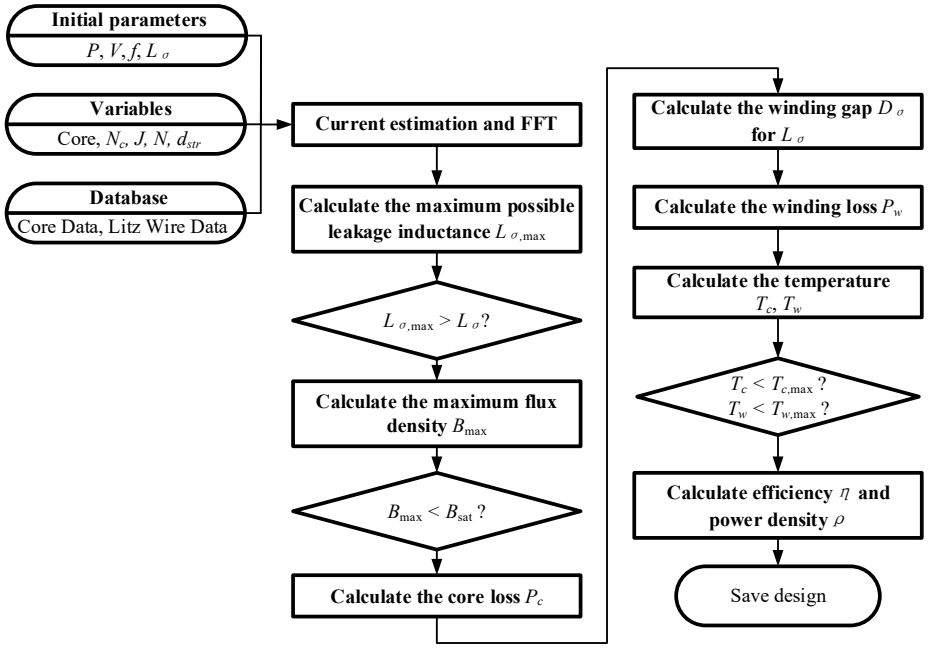

Fig. 6. Flowchart of proposed optimization methodology.

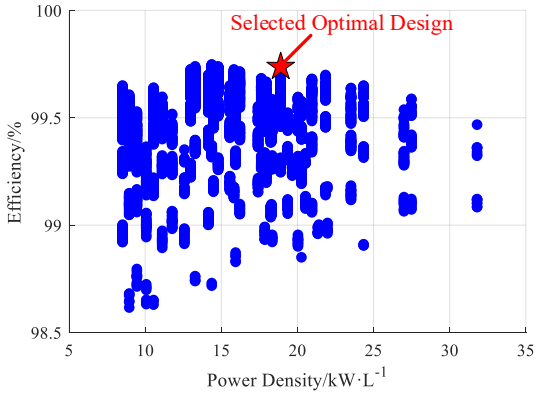

Fig. 7. Pareto optimization results and selected optimal design.

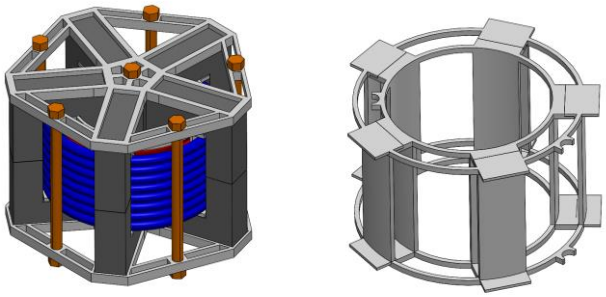
(a) (b)

Fig. 8. The 3-D model of (a) the optimal MCT design and (b) bobbin.

TABLE I. ELECTRIC SPECIFICATIONS OF THE HIGH POWER MCT

Parameter	P	f	V_1	V_2	L_σ
Value	100 kW	50 kHz	1 kV	1 kV	10 μH

TABLE II. KEY PARAMETERS OF THE HIGH POWER MCT

Parameter	Value
Core	Magnetics 0P49930UC × 10
Litz Wire	AWG 38 × 2500
Turns-ratio	8:8

inductance L_σ, and then FFT is used for harmonics component calculation. The models in Section II are adapted for the loss, leakage inductance and temperature estimation. In this optimization algorithm, there exist three conditional judgements: the first one is to compare the maximum possible leakage inductance of the candidate design with the required value, the second one is the avoid the saturation of cores, and the final one is to ensure the temperature rise of the MCT low enough for safety. It is noticed that once the first judgement is satisfied, the accurate winding gap can be calculated to obtain the required leakage inductance, and this geometry parameter is used for the followed winding loss estimation.

Applying the described optimization methodology to the design of a high power MCT with electrical specifications listed in Table I, the result is displayed in Fig. 7. The candidate cores and windings are selected from off-of-shelf ferrite cores and litz wires with strands diameter lower than AWG 35. The key parameters of optimal design is shown in Table II, and the 3-D drawing is illustrated in Fig. 8(a), where two bases are placed on the top and bottom surfaces of

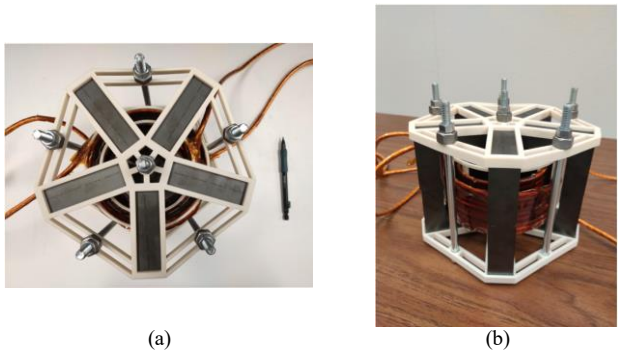
(a) (b)

Fig. 9. (a) The top view and (b) front view of the 100 kW MCT prototype.

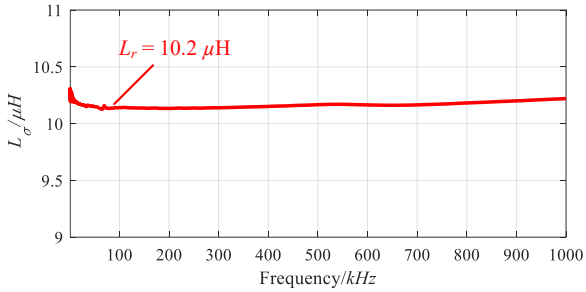

Fig. 10. The measured value of leakage inductance

the cores, and a bobbin for leakage inductance control and airflow channel is designed as shown in Fig. 8(b). The slots of the bases and bobbin are opened to increase heat dissipation.

IV. PROTOTYPE AND TEST

A. Prototype and inductance measurements

The picture of the prototype based on the optimal design is shown in Fig. 9. The bases and bobbin are all 3-D printed with Acrylonitrile Butadiene Styrene (ABS) material. Considering the thickness of inner insulation and outer jacket, the diameter of selected litz wire increases to 6.5mm. The power density of the MCT reaches 17.7 kW/L.

The leakage inductance L_σ is measured by vector network analyzer Bode 100 with the sweep frequency from 1 kHz to 500 kHz, and the result is presented in Fig. 10, which shows the value maintains 10.2 μH with only 2% error compared with the required value.

The magnetizing inductance L_m is measured by open circuit (OC) test. With the square waveform voltage excitation, the measured triangle waveform current as shown in Fig. 11 is generated as the magnetizing current, and the value of L_m can be calculated as

$$L_m = \Delta V \frac{\mathrm{d}t}{\mathrm{d}i} = 2.1mH \tag{12}$$

The L_σ-to- L_m ratio is 4.8%, which is low for eliminating the impact of the magnetizing current on the winding current.

B. Pump-back test

The schematic and setup of the pump-back test for MCT prototype performance verification is shown in Fig. 12. The two H-bridges are made with 1.7 kV silicon carbide (SiC) MOSFETs and low-stray-inductance busbars [18]. The measured voltage and current waveforms at nominal power

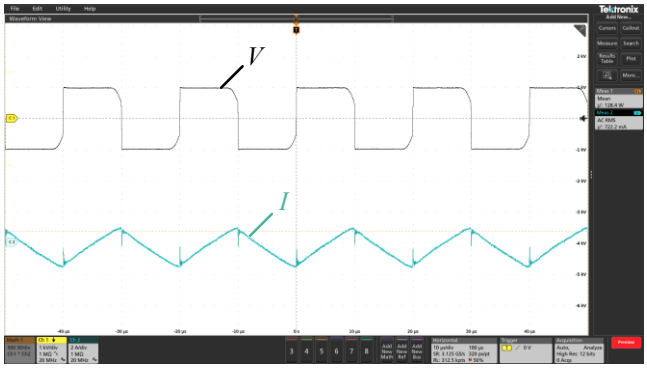

Fig. 11. The voltage and current waveforms of OC test.

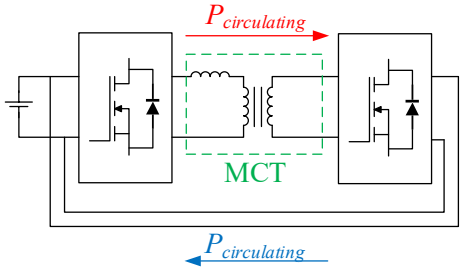

(a)

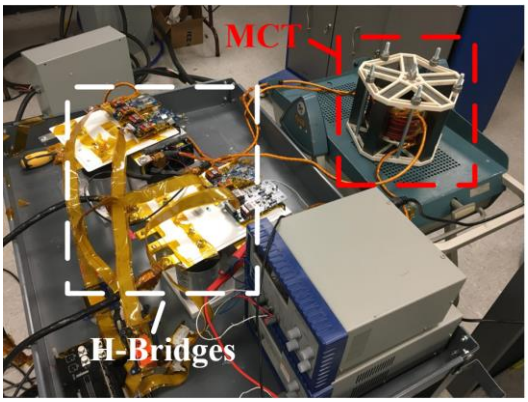

(b)

Fig. 12. (a) The schematic and (b) setup for pump-back test.

operation is displayed in Fig. 13. The RMS current is 142.1 A, which leads to 100 kW and 42 kVar power delivery.

The transformer loss is calculated as

$$P_{\mathrm{MCT}} = P_{\mathrm{total}} - P_{\mathrm{MOSFET}} - P_{\mathrm{busbar}} \tag{13}$$

where P_{total}, P_{MOSFET} and P_{busbar} are the total loss in the system, loss on the SiC MOSFETs, and loss on the busbar, respectively. P_{total} is measured from the DC power supply, P_{MOSFET} is estimated from the curve-fitting function for the switching loss and conduction loss of SiC MOSFETs, and P_{busbar} is estimated with the RMS current and simulated resistance of the high power busbars. With the pump-back test, the efficiency of the MCT under different power levels is measured as shown in Fig. 14. As can be seen that the efficiency reaches the peak value of 99.63% at 80 kW, and the value of 99.62% at 100 kW since the winding loss starts to dominate the transformer loss.

C. Thermal Measurements

The thermal characteristic of the MCT is verified with a 30-min run of pump-back test. The steady-state temperature distribution of the MCT under natural convection is measured as shown in Fig. 15 by thermal camera. The peak

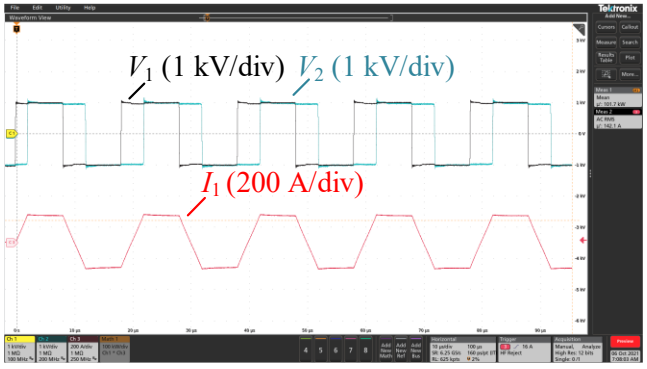

Fig. 13. The voltage and current waveforms of the MCT primary winding at full power operation.

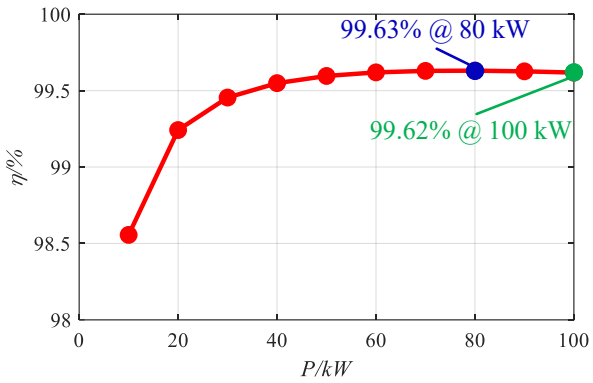

Fig. 14. The efficiency curve of the MCT.

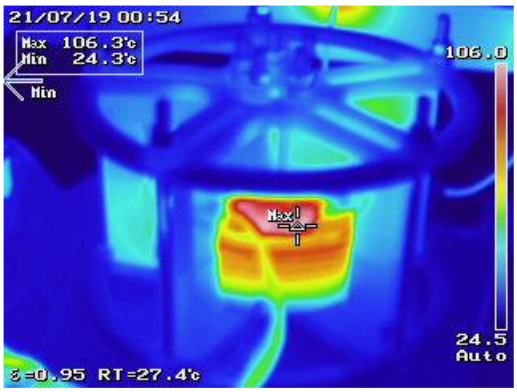

Fig. 15. Steady-state temperature distribution of the MCT after 30 min full power operation.

temperature of windings and cores reaches 106.3°C occurred at the inner primary winding, and 60°C occurred at the area near the IW winding, respectively. Both core and winding temperatures are lower than their corresponding maximum allowed values as 100°C and 125°C.

V. Conclusions

The MCT with improved thermal performance is introduced for high power DAB design. The analytical electrical and magnetic models of MCT for loss and leakage inductance calculation are discussed, and a thermal network, which models the IW winding and OW winding separately, is proposed for temperature rise estimation. An optimization methodology of MCT is illustrated based on the models for high efficiency and high power density transformer design.

A 100 kW/50 kHz MCT prototype with off-of-shelf ferrite cores is built from the optimization results to verify the effectiveness of the presented design process. A 3-D

printed bobbin is designed for both leakage inductance control and air flow cooling. The measured leakage inductance shows high accuracy compared with the required value, and the measured magnetizing inductance is large enough for low magnetizing current. The prototype is tested by the pump-back test from 10 kW to nominal power, and the measured peak efficiency of MCT reaches 99.63%. In addition, the thermal performance of the prototype verifies the improved heat dissipation capability of MCT and shows the available application of MCT on high power SST design.

REFERENCES

[1] X. She, A. Q. Huang, and R. Burgos, "Review of solid-state transformer technologies and their application in power distribution systems," in *IEEE J. Emerg. Sel. Topics Power Electron.*, vol. 1, no. 3, pp. 186-198, Sept. 2013.

[2] D. Rothmund, T. Guillod, D. Bortis, and J. W. Kolar, "99% efficient 10 kV SiC-based 7 kV/400 V DC transformer for future data centers," in *IEEE J. Emerg. Sel. Topics Power Electron.*, vol. 7, no. 2, pp. 753-767, Jun. 2019.

[3] Z. Zhao, Y. Wu, X. Du, and Y. Zhao, "Design and Optimization of the High Frequency Transformer for 100kW *CLLC* Converter," in *Proc. IEEE. Appl. Power Electron. Conf. Expo.*, 2021, pp. 1709-1716.

[4] C. Zhao et al., "Power Electronic Traction Transformer—Medium Voltage Prototype," in *IEEE Trans. Ind. Electron.*, vol. 61, no. 7, pp. 3257-3268, Jul. 2014.

[5] C. G. Dincan et al., "Design of a high-power resonant converter for DC wind turbines," in *IEEE Trans. Power Electron*., vol. 34, no. 7, pp. 6136-6154, Jul. 2019.

[6] B. Zhao, Q. Song, W. Liu, and Y. Sun, "Overview of dual-active-bridge isolated bidirectional DC–DC converter for high-frequency-link power-conversion system," in *IEEE Trans. Power Electron*., vol. 29, no. 8, pp. 4091-4106, Aug. 2014.

[7] B. Zhao, Q. Song, and W. Liu, "Power Characterization of Isolated Bidirectional Dual-Active-Bridge DC–DC Converter With Dual-Phase-Shift Control," in *IEEE Trans. Power Electron*. vol. 27, no. 9, pp. 4172-4176, Sept. 2012.

[8] M. Mogorovic and D. Dujic, "100 kW, 10 kHz medium-frequency transformer design optimization and experimental verification," in *IEEE Trans. Power Electron*., vol. 34, no. 2, pp. 1696-1708, Feb. 2019.

[9] M. Leibl, G. Ortiz, and J. W. Kolar, "Design and Experimental Analysis of a Medium-Frequency Transformer for Solid-State Transformer Applications," in *IEEE J. Emerg. Sel. Topics Power Electron.*, vol. 5, no. 1, pp. 110-123, Mar. 2017.

[10] Z. Guo, R. Yu, W. Xu, X. Feng, and A. Q. Huang, "Design and optimization of a 200-kW medium-frequency transformer for medium-voltage SiC PV inverters," in *IEEE Trans. Power Electron*., vol. 36, no. 9, pp. 10548-10560, Sept. 2021.

[11] D. Rothmund, G. Ortiz, T. Guillod, and J. W. Kolar, "10kV SiC-based isolated DC-DC converter for medium voltage-connected solid-state transformers," in *Proc. IEEE. Appl. Power Electron. Conf. Expo.*, 2015, pp. 1096-1103.

[12] K. Venkatachalam, C. R. Sullivan, T. Abdallah, and H. Tacca, "Accurate prediction of ferrite core loss with nonsinusoidal waveforms using only Steinmetz parameters," in *Proc. IEEE Workshop Comput. Power Electron.*, Jun. 2002, pp. 36-41

[13] P. L. Dowell, "Effects of eddy currents in transformer windings," *Proc. Inst. Electr. Eng.*, vol. 113, no. 8, pp. 1387–1394, Aug. 1966.

[14] R. P. Wojda and M. K. Kazimierczuk, "Winding resistance and power loss of inductors with litz and solid-round wires," in *IEEE Trans. Ind. Appl.*, vol. 54, no. 4, pp. 3548-3557, Jul.-Aug. 2018.

[15] Z. Ouyang and M. A. E. Andersen, "Overview of planar magnetic technology—Fundamental properties," in *IEEE Trans. Power Electron*., vol. 29, no. 9, pp. 4888-4900, Sept. 2014.

[16] Z. Ouyang, J. Zhang, and W. G. Hurley, "Calculation of leakage inductance for high-frequency transformers," in *IEEE Trans. Power Electron*., vol. 30, no. 10, pp. 5769-5775, Oct. 2015.

[17] Bergman, Theodore L., et al. *Fundamentals of heat and mass transfer.* John Wiley & Sons, 2011.

[18] Y. Wu et al., "A 150-kW 99% efficient all silicon carbide triple-active-bridge converter for solar-plus-storage systems," in *IEEE J. Emerg. Sel. Topics Power Electron.*, doi: 10.1109/JESTPE.2020.3044572